Applied Catalysis B: Environmental 225 (2018) 100–109

Contents lists available at ScienceDirect

Applied Catalysis B: Environmental

journal homepage: www.elsevier.com/locate/apcatb

Composite $H_3PW_{12}O_{40}$–TiO_2 catalysts for toluene selective photo-oxidation

Guillermo R. Bertolini[a], Luis R. Pizzio[a], Anna Kubacka[b], Mario J. Muñoz-Batista[b,*], Marcos Fernández-García[b,*]

[a] Centro de Investigación y Desarrollo en Ciencias Aplicadas "Dr. J. Ronco", CINDECA-CCT La Plata-CONICET-UNLP, Calle 47 N° 257, 1900, La Plata, Argentina
[b] Instituto de Catálisis y Petroleoquímica, CSIC, C/Marie Curie, 2, 28049 Madrid, Spain

ARTICLE INFO

Keywords:
HBA
titania
UV
Sunlight
Toluene
photonic efficiency

ABSTRACT

A series of composite systems based on titania and growing quantities of tungstophosphoric acid are prepared and characterized using infrared, nuclear resonance, UV–visible, photoluminescence, and photoelectron spectroscopies, transmission electron microscopy as well as x-ray diffraction and porosimetry techniques. These techniques showed evolution of the tungstophosphoric acid species supported into titania while this majority component of the system suffers minor changes. The activity and stability of the composite samples for gas phase toluene photo-oxidation under UV and sunlight-type irradiation conditions was measured by means of the reaction rate and the photonic efficiency parameter. The modeling of the radiation field was accomplished by numerically solving the radiative transfer equation. The photo-activity of the composite materials showed a significant selectivity towards the transformation of the hydrocarbon into a partially oxidized product, benzaldehyde. Both the activity and selectivity of the titania are significantly affected by the presence of tungstophosphoric acid species. The physico-chemical characterization was able to point out to the leading role of specific polytungstate species in driving the enhancement of the activity and selectivity of the reaction, rendering stable, highly active and selective photo-catalysis.

1. Introduction

Heterogeneous photocatalysis is an advanced oxidation process that uses semiconductors broadly applied in the degradation and transformation of organic pollutants [1,2], production of hydrogen using light and bio-molecules [3], conversion of CO_2 into high value-added industrial chemicals and hydrocarbon fuels [4,5] as well as degradation of biological microorganisms [6].

One family of materials potentially interesting corresponds to the Polyoxometallates (POMs). POMs correspond to a wide class of functional materials consisting on nanoscale transition metal oxide clusters [7]. The most explored POMs are the heteropolyacids (HPAs); they are customarily classified starting from the unit "parent" polycations, being the Keggin ($XM_{12}O_{40}^{n-}$), Dawson ($X_2M_{18}O_{62}^{n-}$), Lindquist ($M_6O_{19}^{n-}$), and Anderson ($XM_6O_{24}^{n-}$) structures among the most utilized as functional materials in chemistry [7,8]. The Keggin anions contain a heteroatom X (X = P, Si) as the center of a XO_4^{n-} unit and the so-called addenda atom, commonly W or Mo, constructing the external coordination shell of the unit. In particular, the heteropolyacid $[PW_{12}O_{40}]^{3-}$ anion displays a size of ca. 1 nm and consists on a PO_4^{3-} tetrahedron surrounded by four W_3O_9 groups formed by edge-sharing octahedra. Heteropolyacids with Keggin structure are strongly acidic and present significant stability when supported on high surface area oxides [8–10].

Among Keggin heteropolyacids functional uses, homogeneous but particularly heterogeneous photocatalysis have emerged as a field of intense research. The combination with titanium oxide corresponds to the most widely analyzed photo-catalytic combination [8–13]. Apart from introducing new acidic and cationic functionalities to a titania support, the photocatalytic properties of the composite material can be improved (with respect to the titania or heteropolyacid single references) not only by a simple effect of the heteropolyacid dispersion (and thus increase of potential active sites availability to reactants) but also as a fact that the Keggin structure can behave itself as a photocatalyst upon light excitation of the so-called oxygen-to-metal charge transfer. Excited Keggin polytungstate anions correspond to strong oxidant species compared with their electronic ground state due to the higher energy of the corresponding electronic levels. In addition, excitation of this material allows a more efficient use of visible light with respect to titania alone materials [8–11]. As a result of the fitness of the above mentioned physico-chemical properties for functional use in photocatalytic processes, improved performance with respect to titania counterparts in photo-degradation of organic compounds has been frequently reported under UV and/or visible light illumination

* Corresponding authors.
E-mail addresses: mario.munoz@icp.es, jmunoz385x@gmail.com (M.J. Muñoz-Batista), mfg@icp.csic.es (M. Fernández-García).

https://doi.org/10.1016/j.apcatb.2017.11.055
Received 14 September 2017; Received in revised form 30 October 2017; Accepted 21 November 2017
Available online 22 November 2017
0926-3373/

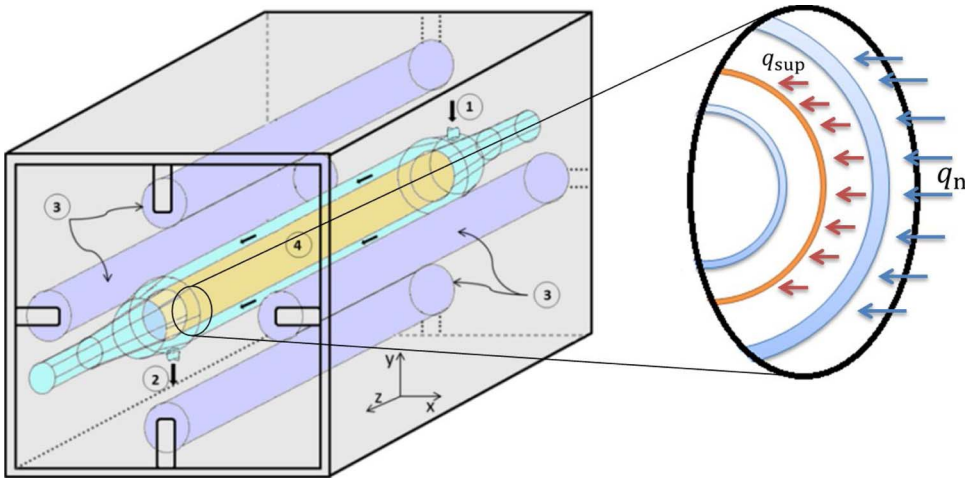

Fig. 1. Photocatalytic annular reactor. (1) gas inlet, (2) gas outlet, (3) lamps, (4) catalyst sample.

[8,11,14–19]. Less common is however the use of heteropolyacids-titania composites in selective photo-transformations. Nevertheless, as a representative example we can highlight the work of García-López et al. in 2-propanol photo-assisted (or photo-thermal) catalytic dehydration, a reaction facilitated by the acidity of the composite system [20].

Here we presented a study of the evolution of the toluene selective photo-oxidation to benzaldehyde through a series of samples having different surface concentration of the heteropolyacid as a benmarch test. Photo-catalytic production of benzaldehyde has been attempted from benzyl alcohol [21], but the achievement of such reaction starting from the corresponding hydrocarbon would be significantly more appealing from an economical point of view. As detailed in this contribution, almost complete selectivity towards to partial oxidation can be obtained using composite $H_3PW_{12}O_{40}$–TiO_2 composite catalysts. The complete physico-chemical characterization of the materials using X-ray diffraction, UV–visible, photoluminescence, X-ray photoelectron, infrared and nuclear magnetic spectroscopies together with microscopy would allow to rationalize the result as a function of the polytungstate species present at the titania surface, their electronic and structural effects in the support properties as well as the composite material as a whole.

2. Experimental

2.1. Preparation of the samples

A titanium isopropoxide (Aldrich, 26.7 g) solution was prepared in absolute ethanol (Merck, 186.6 g) under N_2 atmosphere and at room temperature, continuously stirring for 10 min. Then, 0.33 mL of a 0.28 M HCl aqueous solution was slowly added in order to catalyze the sol–gel reaction. After 3 h, 120 g of a urea–ethanol– water (1:5:1 w/w) solution was added, to act as a mesoporous forming agent, together with an ethanol solution of tungstophosphoric acid ($H_3PW_{12}O_{40}$. $23H_2O$, Fluka p.a.) under vigorous stirring. The amount of TPA was varied with the purpose of obtaining a TPA concentration of 10, 20 and 30% by weight in the final solid (named TiO_2 for the reference and TiO_2 TPA10, TiO_2 TPA 20, and TiO_2 TPA30, respectively). The gels were dried at room temperature and the solids were ground into powder and extracted with distilled water for three periods of 24 h, in order to remove the urea. Finally, the solids were thermally treated at 500 °C for 2 h.

2.2. Characterization techniques

The Brunauer – Emmett – Teller (BET) surface areas and average pore volumes and sizes were measured by nitrogen physisorption (Micromeritics ASAP 2010). XRD profiles were obtained with a Seifert D-500 diffractometer using Ni-filtered Cu Kα radiation with a 0.02° step and fitted using the Von Dreele approach to the Le Bail method [22]; particle sizes and microstrain were measured with XRD using the Willianson–Hall formalism. FT-IR spectra of the supports and catalysts were obtained in the 400–4000 cm^{-1} wavenumber range using Bruker IFS 66 FT-IR spectrometer and pellets in KBr. The 31P MAS-NMR spectra were recorded using the CP/MAS 1H–31P technique with Bruker Avance II equipment. A sample holder of 4 mm diameter and 10 mm in height was employed, using 5 μs pulses, a repetition time of 4 s and working at a frequency of 121.496 MHz for 31P at room temperature. The spin rate was 8 kHz and several hundred pulse responses were collected. Phosphoric acid 85% was employed as external reference. UV–vis diffuse-reflectance spectroscopy experiments were performed on a Shimadzu UV2100 apparatus using nylon as a reference. XPS data were recorded on 4 × 4 mm^2 pellets, 0.5 mm thick, prepared by slightly pressing the powered materials which were outgassed in the prechamber of the instrument at room temperature up to a pressure $< 2 \times 10^{-8}$ Torr remove chemisorbed water from their surfaces. The SPECS spectrometer main chamber, working at a pressure $< 10^{-9}$ Torr, was equipped with a PHOIBOS 150 multichannel hemispherical electron analyzer with a dual X-ray source working with Ag Kα ($h\nu$ = 1486.2 eV) at 120 W, 20 mA using C 1 s as energy reference (284.6 eV). Transmission electron microscopy (TEM) and X-ray energy dispersive spectra (XEDS) were recorded on a JEOL 2100F TEM/STEM microscope using a copper sample holder (Lacey/Carbon 200 Mesh, Copper (Cat. # LC200-CU) from Electron Microscopy Science – emsdiasum). Photoluminescence spectra were measured at room temperature on a Fluorescence Spectrophotometer (Perkin Elmer LS50B).

3. Photo-catalytic experiments

Gas-phase photo-oxidation of toluene (Aldrich, spectroscopic grade) were carried in a continuous flow annular photoreactor (Fig. 1) and using a set-up described elsewhere [23,38]. Table 1 shows details of reactor configuration and experimental conditions. Activity and selectivity for the gas-phase photooxidation were tested in a continuous flow annular photoreactor containing ca. 40 mg of photocatalyst as a thin layer coating on a pyrex tube. The corresponding amount of catalyst was suspended in 1 mL of ethanol, painted on a pyrex tube (cut-off at ca. 290 nm), and dried at RT. The reacting mixture (100 ml min^{-1}) was prepared by injecting toluene (≥99%; Aldrich) into a wet (ca. 75% relative humidity) 20 vol.% O_2/N_2 flow before entering to the photoreactor, yielding an organic inlet concentration of ca. 700 ppmv. After flowing the mixture for 6 h (control test) in the dark, the catalyst was irradiated by four fluorescent daylight lamps (6W, Sylvania F6W/D) with a radiation spectrum simulating sunlight (UV content of 3%; main emission lines at 410, 440, 540, and 580 nm, symmetrically positioned

Table 1
Geometrical parameters of the reactor and experimental Operating Conditions.

Parameter (unit)	Value
No. of lamps	4
Lamp length (cm)	19
Lamp radius (cm)	0.8
Reactor length (cm)	15
Reactor Inner radius (cm)	0.8
Reactor Outer radius (cm)	1.2
Feed flow rate ($cm^3\ min^{-1}$)	100
Temperature (°C)	30
Pressure (atm)	1
Toluene concentration (ppm)	700
Relative humidity (%)	90

outside the photoreactor. Similar tests were carried out using UV lamps (Sylvania F6WBLT-65; 6 W, maximum at ca. 350 nm). Reaction rates were evaluated under steady-state conditions, typically achieved after 10 h from the irradiation starting. The concentration of reactants and products was analyzed using an on-line gas chromatograph (Agilent GC 6890) equipped with HP-PLOT-Q/HP-Innowax columns (0.5/0.32 mm I.D. × 30 m) and TCD (for CO_2 measurement)/FID (organic measurement) detectors. Carbon balance above 95% was obtained in all experiments.

4. Photonic efficiency calculation

According to the IUPAC recommendation, the photonic efficiency (also called apparent quantum efficiency) is defined as Eq. (1) [24].

$$\text{AppQE} = \frac{r(\text{mol m}^{-2}\text{s}^{-1})}{\langle q_{sup}\rangle(\text{Einstein m}^{-2}\text{s}^{-1})} \times 100 \quad (1)$$

Where: r is the reaction rate normalized by catalytic area and q_{sup} is the radiation flux within a defined wavelength interval inside the irradiation window of the reactor. Besides, the IUPAC emphasizes that "the incident number of photons (prior to absorption) should be used" in Eq. (1). In this contribution we use the two most usual interpretations considering the annular reactor here used. The first one considers q_{sup} as the radiation flux measurable inside the irradiation window of the reactor (external glass). In this case, it is only necessary to know the photon flux emitted by the lamp and the distribution of the emitted energy together with the glass optical properties. Using this approach we obtained values of 1.55×10^{-8} and 5.2×10^{-8} Einstein $cm^{-2}\ s^{-1}$ for ultraviolet (UV) and sunlight-type (ST) irradiation conditions.

Note that, although many contributions use this value, which can be measured experimentally, the calculation of the radiation flux impinging on the catalytic film implies a complete analysis of the light-matter interaction in the reaction system. This corresponds to an alternative measurement of the apparent quantum efficiency of significance considering our reactor geometry. The corresponding justification of the calculation procedure and the efficiency results are presented in the Supporting Information section.

5. Results and Discussion

5.1. Characterization results

The X-ray diffraction patterns of the composite samples (TiO_2 TPA10, TiO_2 TPA20, and TiO_2 TPA30) and bare titania (TiO_2) sample are displayed in Fig. 2. The bare titania reference shows a diffraction pattern dominated by the anatase phase (PDF 21-1272; space group $I4_1/amd$). As it was reported previously, calcination below 600 °C typically renders a highly crystalline pure anatase phase for the majority of the preparation methods used (sol-gel, microemulsion, chemical vapor deposition, etc.) [25]. Here, we obtained the anatase polymorph

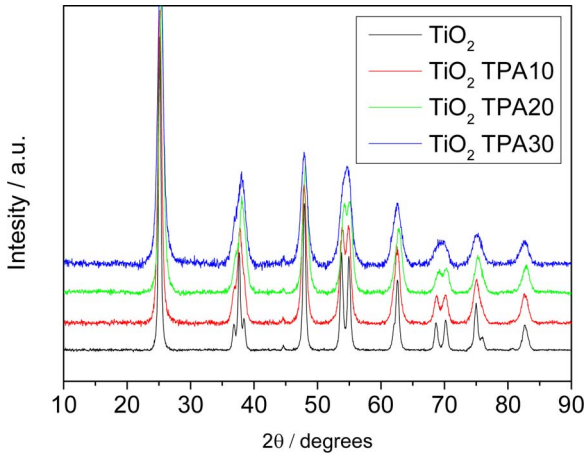

Fig. 2. XRD patterns for the TiO_2 TPA (X) samples and Ti reference.

with a crystallyte size of 14–16 nm. The modification of titania with tungstophosphoric acid, retarded the crystallization and stabilized TiO_2 in anatase phase, as can be inferred by the larger broadening of the titania oxide peaks in TiO_2-TPA XRD patterns. The XRD patterns of TiO_2 TPA10, TiO_2 TPA 20, and TiO_2 TPA 30 samples (Fig. 2) show the influence of TPA content on the crystallinity of the samples. The crystallinity increases in parallel with the decrease of the TPA content. It can be clearly see, for example, that as result of the TPA content decrement, the wide peak at 54.6° splits into two peaks at 53.8° (105) and 54.9° (211). The same behavior is shown by the peak at 69.5° that split into two peaks at 68.7° (116) and 70.1° (220). The corresponding anatase crystal size decreases by ca. 2 nm with respect to the parent material (see Table 2).

The stabilization effect by the surface deposition of the polytungstate has been previously mentioned in the literature [26,27]. On the other hand, the XRD profiles do not show diffraction lines assigned to crystalline heteropolyacid species. The surface area of titania reference presents a value of 33.2 $m^2\ g^{-1}$ while the subsequent addition of tungstophosphoric acid for the binary samples does not significantly modify it. This result suggests that the surface area is dominated by the major (by weight) titania component. This conclusion is also valid for interpreting other morphological properties summarized in Table 2, in which only limited variation(s) of pore volume and pore size are observed through the series.

The structural properties of composite materials were also analyzed with the help of microscopy. TEM micrographs for the four samples studied are presented in Fig. 3. The figure presents low magnification views of the catalysts and high-resolution micrographs for each sample. The micrographs allow visualizing the TiO_2 crystallinity without significant differences throughout the sample series. Even though identification of keggin structure is rather complex in Fig. 3, the contact between the heteropolyacid and TiO_2 have been confirmed by XEDS (Fig. S7 and Table S1 of the SI summarize the information concerning the XEDS analysis). Fig. S8 shows the elemental composition of composite materials and Table S1 the average atomic weight % obtained at

Table 2
Morphological properties for the Ti reference and the samples.[a]

Sample	BET surface area (m^2/g)	Pore volume (cm^3/g)	Pore size (nm)	Anatase particle size (nm)	Band Gap (eV)
TiO_2	33.2	0.065	6.42	16.1	3.2_5
TiO_2TPA10	28.4	0.048	5.85	14.7	3.1
TiO_2TPA20	29.9	0.050	4.91	14.7	3.1
TiO_2TPA30	35.5	0.069	5.92	14.1	3.1

[a] Average Standard error: BET area: 1.5 $m^2\ g^{-1}$; pore size 7%, band gap: 0.03 eV.

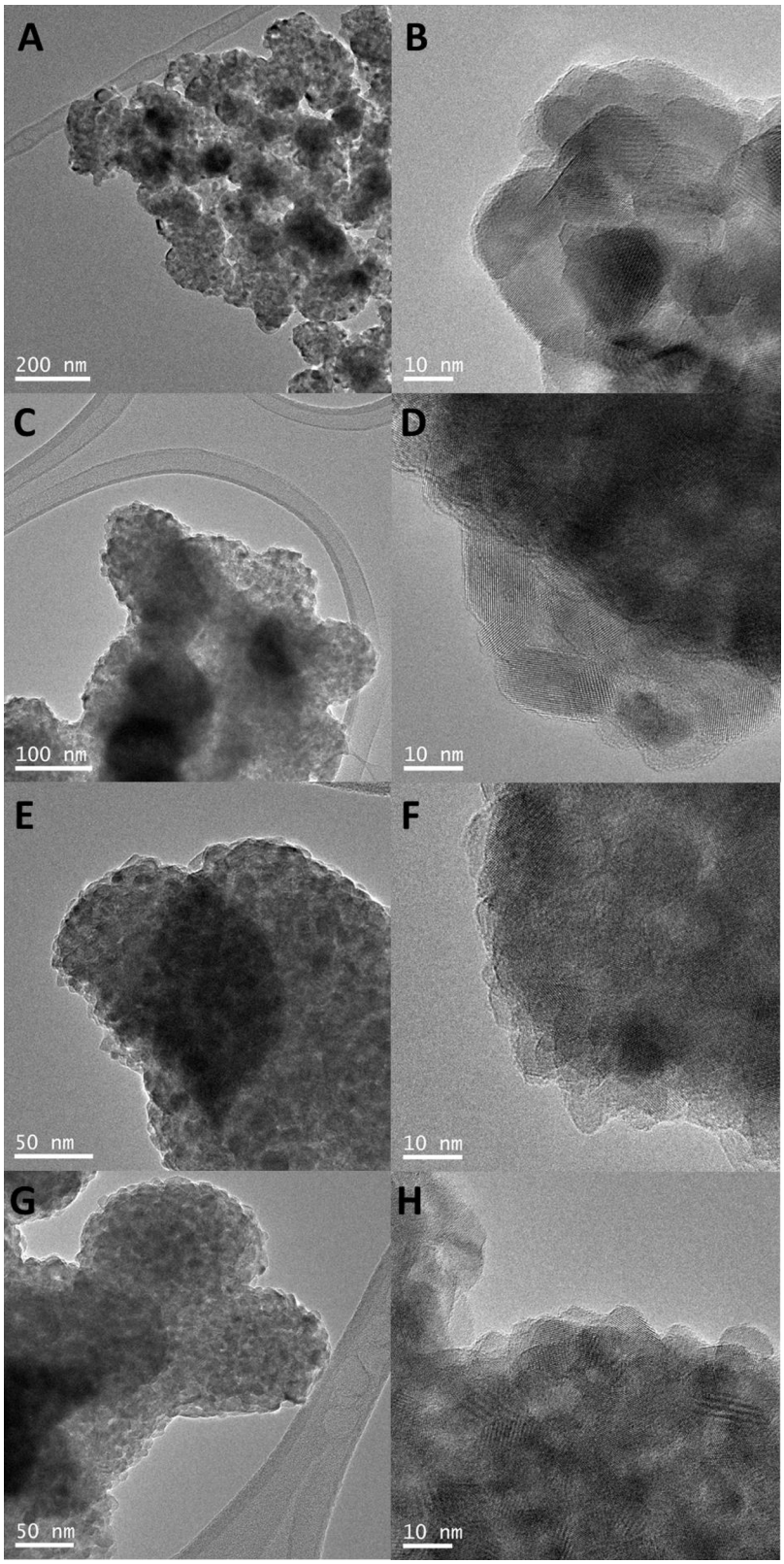

Fig. 3. TEM images of the TiO_2 reference (A-B), TiO_2-TPA10 (C-D), TiO_2-TPA20 (E-F) and TiO_2-TPA30 (G-H) samples.

several (ca. 50 per sample) positions of the catalytic solids. XEDS analysis is in rough agreement with the theoretical weight % of the composite materials and provides evidence of the heterogeneity of the surface deposition of the heteropolyacid species onto the titania surface.

To obtain more information of the polytungstate surface species of the composite materials we carried out a multitechnique, spectroscopic examination of the catalysts. Starting from UV-visible spectroscopy, we can obtain information on both the titania and polytungstate components of the catalysts. The UV-visible spectra (Fig. 4) are dominated by the titania counterpart as a result of its larger (in fact dominant) molar contribution of this component in the materials. Considering that

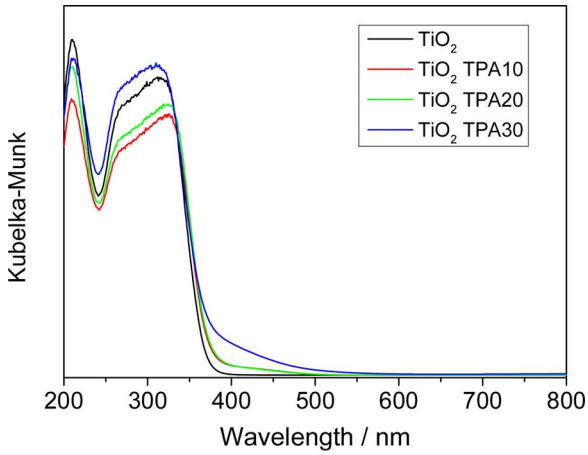

Fig. 4. UV–vis for the TiO_2 TPA (X) samples and Ti reference.

titania is an indirect band gap semiconductor [28], we obtained the band gap values included in Table 2. A modest decrease of ca. 0.1 eV is observed for all composite samples with respect to the bare anatase. The rough constancy of the band gap energy among composite samples is evident, indicating that the electronic properties of the support do not suffer a significant modification by the presence of the tungstophosphoric component. At higher wavelengths of the titania sigmoidal decay, characteristic of the band gap, we observed a broad shoulder extending from ca. 400 to 520 nm. This is characteristic of the polytungstate, which has optical transitions assigned to the charge transfer from bridging (W-O-W) or terminal (W-O_d) O 2p to W 5d electronic states [29]. The latter, terminal species may contribute to the shoulder mentioned, although it appears also related to the interaction of W and Ti species, as previously claimed [30].

The electronic information about the catalysts components was completed with the help of X-ray photoelectron spectroscopy. Fig. 5 summarizes results concerning the W 5d, Ti 2p and P 1 s XPS peaks. W and Ti peaks do not show significant alteration among the samples and correspond in both cases to single oxidation states. These oxidation states are W(VI) and Ti(IV) according to their binding energies of, respectively, 247.2 and 458.3 eV [31–33]. The P 1s peak shows a main contribution at ca. 133.0 eV with a significant broadening which appears to grow as the content of the polytungstate content of the materials grows. Although the important noise of the spectra does not allow a detailed analysis of the P 1s peak, it is clear that the peak width of P increases significantly with polytunsgtate content, reflecting some heterogeneity in the local environment of the atom. Such heterogeneity grows, as mentioned, with the polytunsgtate content of the catalyst and would be a consequence of the UV-visible-detected interaction between the two components of the materials.

To further progress on the study of such heterogeneity of the samples, they were analyzed with infrared and ^{31}P NMR spectroscopies. Infrared spectra are collected in Fig. 6 for the relevant region between 1400 and 400 cm^{-1}. The plot includes results from the composite samples as well as the bare TiO_2, polytungstate and the sodium salt of the lacunary anion. The $[PW_{12}O_{40}]^{3-}$ spectra displays bands at at 1081, 982, 888, 793, 595, and 524 cm^{-1}, assigned to the stretching vibrations P—O_a (a subindex indicating oxygen bridging W and P atoms), W—O_d (d subindex indicating terminal atoms), W—O_b—W (b subindex indicating corner sharing atoms), W—O_c—W (c subindex indicating edge sharing atoms), and to the bending vibration O_a—P—O_a, respectively. The sodium salt of the lacunary ion $[PW_{11}O_{39}]^{7-}$ shows bands at 1100, 1046, 958, 904, 812, and 742 cm^{-1}, in agreement with the literature [34]. Anatase (titania reference) presents increasing absorbance in the wavenumber region below 800 cm^{-1}, a fact related to the activation of lattice collective vibrations [35]. The IR spectra of the composite samples present the same peaks in the 400–1400 cm^{-1} region but with intensity clearly correlated with the polytungstate concentration. We can distinguish the most intense 1081, 982, and 888 contributions of the $[PW_{12}O_{40}]^{3-}$ reference spectrum in all composite sample infrared spectra. In addition we can observe a series of peaks correlated with the 1100, 1046, 958, and 812 cm^{-1} contributions of the lacunary ions but with a red shift of ca. 20 cm^{-1}. The latter contribution appears of more importance as the polytungstate content grows in the composite materials. The IR study thus suggests that the contact with the anatase phase alters significantly a fraction of the surface polytungstate anions.

Finally, ^{31}P MAS-NMR spectra of the composite samples are displayed in Fig. 7. For the lower content of the polytungstate at the composites two lines at −14.5 and 12.1 ppm are detected. These correspond to the $[PW_{12}O_{40}]^{3-}$ and the dimeric $[P_2W_{21}O_{71}]^{6-}$ species, respectively [36]. They display a downfield shift and slight line width increase as compared with the bulk contributions; both facts attributed to the interaction with the anatase support [37]. The ^{31}P MAS-NMR spectra of the remaining composite samples showed an additional contribution at 10.7–10.8 ppm assigned to the $[PW_{11}O_{39}]^{7-}$ anion [36,37]. As may be expected by the polytungstate content of the materials, the $[PW_{12}O_{40}]^{3-}$ is the dominant species for all cases.

In summary, the multitecnique approach indicates that the heterogeneity of the polytungstate species grows with its content at the composite materials, as described previously [29]. The unperturbed (or minimally modified by effect of the titania) $[PW_{12}O_{40}]^{3-}$ anion is the dominant species at the anatase surface, with the dimeric $[P_2W_{21}O_{71}]^{6-}$ species accompanying to the unperturbed one. For loadings above 10 wt. %, the additional presence of the $[PW_{11}O_{39}]^{7-}$ anion is detected. The evolution of the anion at the surface is likely due to the limited stability of the $[PW_{12}O_{40}]^{3-}$ anion in solution. On passing we note that the main FT-IR bands of the dimer $[P_2W_{21}O_{71}]^{6-}$, assigned to the stretching vibrations P—O, W—O, W—O—W appear at wavenumber values similar to those characteristic of the $[PW_{12}O_{40}]^{3-}$ anion, so their presence cannot be confirmed based on FT-IR results only [29], but are clearly observed in the NMR spectra. In contrast to the polytungstate species, anatase displays limited evolution; only a stabilization of the primary particle size of the oxide becomes evident.

5.2. Catalytic results

The reaction rates measured for toluene photo-oxidation reaction are presented in Fig. 8. The pure anatase (titania) sample shows results comparable with previous ones corresponding to anatase-dominated samples [29]. The presence of the polytungstate at the surface renders a positive effect over the reaction rate in all conditions tested, i.e. for all polytungstate loadings and under all illumination conditions measured. The maximum of activity is obtained for the sample having a 20 wt. % of the polytungstate component, presenting an enhancement ratio with respect to the bare titania of 2.6 and 3.5 for, respectively, UV and sunlight-type illumination conditions. This pure titania is also more active than the commercial P25 reference reported previously using the same setup of this work [33]. From the activity level shown by the sample with a 20 wt. %, there is a decay of activity although such decay is less marked than the one observed at the other side of the volcano-type plot presented by the activity.

In this work, we also carry out a stability test for the most active sample (TiO_2 TPA 20). The results presented in Fig. 9 show that no significant catalyst deactivation occurred after 3 cycles reaction (1 cycle = 24 h of reaction). This stability in the photochemical process is consistent with the characterization results for the spent sample, carried out using UV–vis, XRD, TEM-EDX and XPS (data presented in Figs. S8–S10 and Table S2 of the supporting information). According to the XRD results (Fig. S9A), the anatase TiO_2 dominant phase does not suffer significant modifications. Likewise, no modification of the band gap energy was detected with respect to the fresh sample. The small modifications of the UV–vis spectra (Fig. S8A) could correspond to carbon deposition during the photocatalytic reaction. Moreover and according

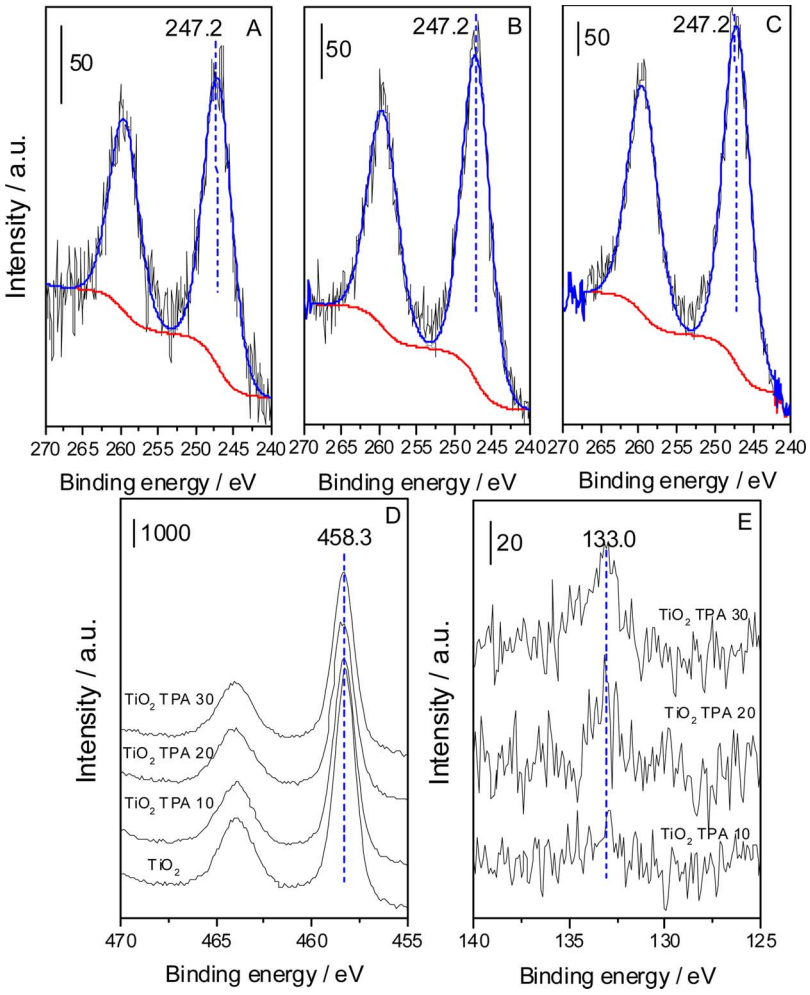

Fig. 5. W 4d XPS spectra of the TiO_2 TPA10 (A), TiO_2 TPA20 (B) and TiO_2 TPA30 (C) sample, respectively. (D) Ti 2p XPS spectra of the TiO_2 TPA(X) samples and Ti references. (E) P 2p XPS spectra of the TiO_2 TPA(X) samples.

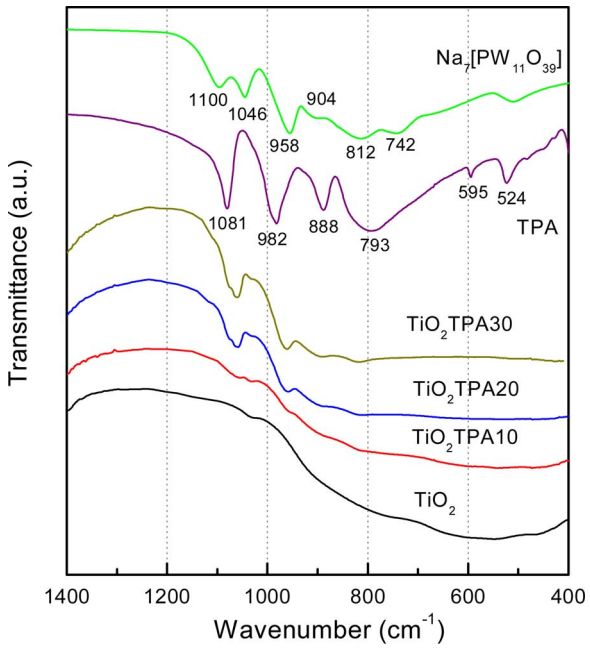

Fig. 6. Infrared spectra of the composite and reference materials (bulk TPA and $Na_7[PW_{11}O_{39}]$).

to both TEM and EDX analysis (Fig. S9 and Table S2), the TiO_2 and TPA components do not suffer significant structural modifications. Additional information concerning the chemical oxidation state can be obtained from the XPS study displayed in Fig. S10. Rather similar Ti 2p, W4d and P 2p spectra were obtained from fresh and used TiO_2 TPA20 sample.

In Fig. 8 we present also the photonic (apparent quantum) efficiency calculated using Eq. (1) and following the methodology described above. The photonic efficiency renders maximum values of the apparent quantum efficiency of ca. 8.8×10^{-4} and 2.3×10^{-4} upon UV and sunlight-type illumination, respectively. The lower values are usually obtained (mainly under sunlight-type irradiation), as i) some visible photons do not have enough energy to create electron-hole pairs (due to the electronic of the systems which, in our case, display near null absorption above ca. 550 nm, see Fig. 4) and/or ii) a fraction of the charge carrier pairs generated have not enough energy to activate efficiently the toluene molecule. The photonic efficiencies are relatively inferior to those presented, for example, by chemically-related, composite binary samples containing tungsten as (oxide-type) surface species or doping cations of the anatase phase in the photo-oxidation of toluene [23,33,38].

Selectivity of toluene photo-oxidation is presented in Fig. 10. The photo-oxidation of toluene render typically benzaldehyde as partial oxidation product and carbon dioxide as total oxidation one [23,33,39,40,41]. Interesting to remark is the fact that the hydrocarbon photo-oxidation is carried out here within a continuous (experiment presented consider 24 h of contact time), gas-phase scheme at room temperature and pressure and using oxygen from air (20% concentration) as oxidant species. This together with the facile separation/regeneration/reutilization of the catalysts (not usually accomplished in

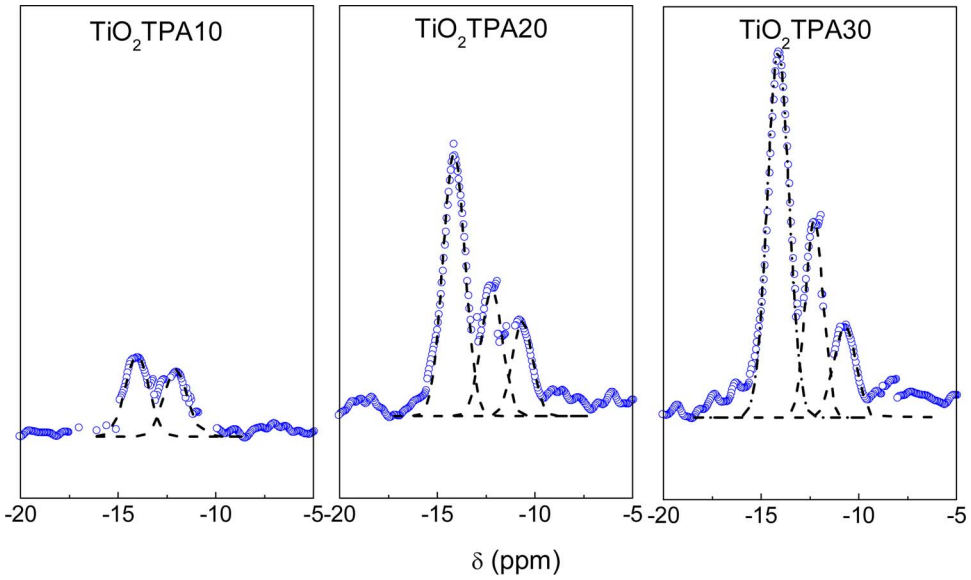

Fig. 7. ^{31}P MAS–NMR spectra of the TiO_2 TPA (X) samples. Fitting results of the different P-containing species are presented.

liquid phase processes, particularly if titania P25 is used as photo-catalyst) would provide an optimum base for the applicability of a selective photo-oxidation process if high selectivity is reached. Fig. 10 displays that the titania reference shows significant contributions of both products. The production of the partial oxidation product increases under sunlight-type illumination as the production of the total oxidation product, carbon dioxide, requires a significantly larger number of charge carriers (in fact a factor of 9, see Ref. [42] for details), which are likely less available upon illumination with less energetic photons. Additionally, in presence of the tungstate component, the opening of

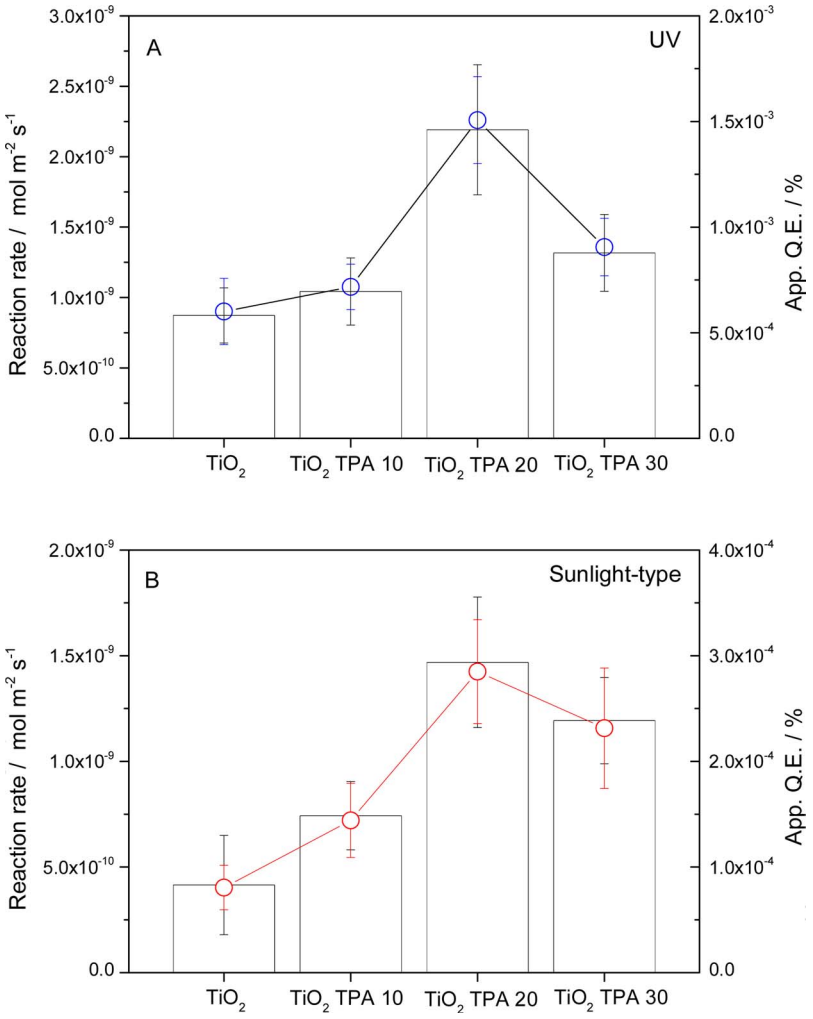

Fig. 8. Reaction rate (columns) and apparent quantum efficiency (circles) under UV (A) and sunlight-type (B) irradiation conditions.

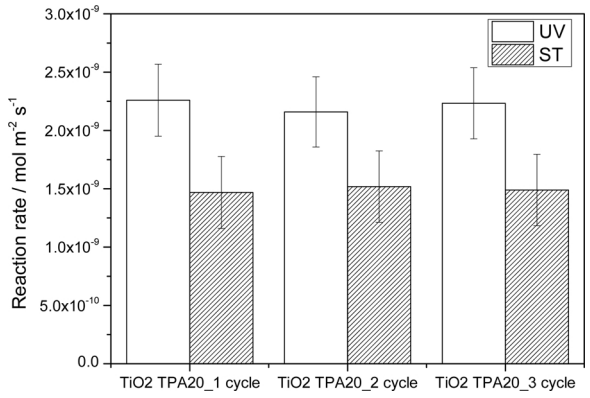

Fig. 9. Toluene photo-oxidation reaction rate for the most active sample (TiO_2 TPA 20) during 3 cycles of reaction. See details in the main text.

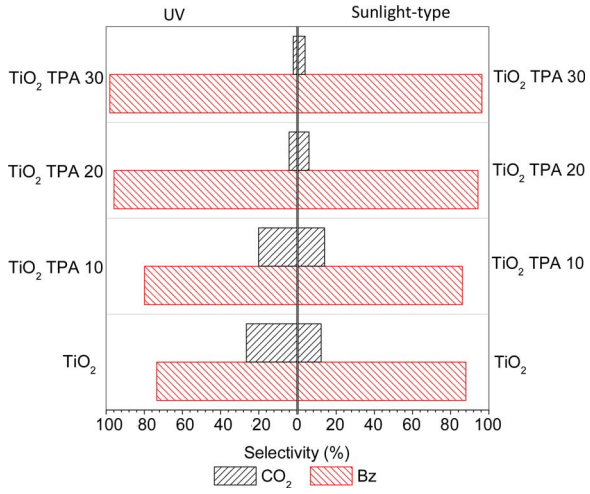

Fig. 10. Selectivity to CO_2 and Benzaldehyde (Bz) for the Ti reference and TiO_2 TPA(X) samples.

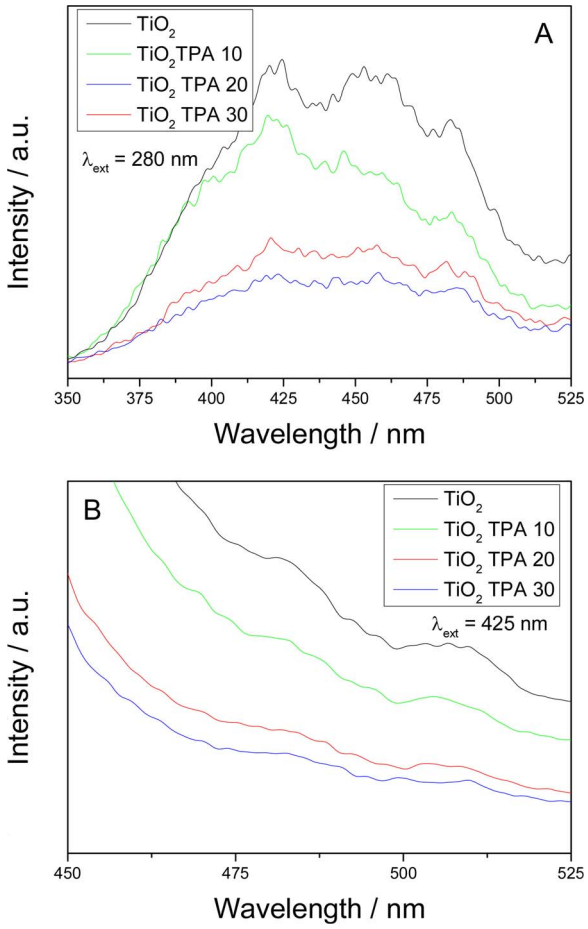

Fig. 11. Photoluminescence spectra of the samples under UV (A) and Visible (B) excitation.

the oxygen capture channel (previously discussed upon absorption of visible photons) may alter the role of the oxidant species at the reaction, favoring not only activity but also (and to a moderate degree) the production of the partial oxidation product. Note that the selectivity of benzaldehyde is as higher as 96% for the catalyst showing optimum activity upon all illumination conditions. This selectivity is higher than those previously reported in the literature for W-promoted anatase materials [23,33,38], and provides evidence of the goodness of the composite catalysts in the selective oxidation of toluene to benzaldehyde.

An important point to discuss is, nevertheless, the enhancement of the activity with respect to a highly active anatase reference, which is attributed to the different beneficial effects of the interface contacts between the two components of the materials. The interface contact mentioned has been demonstrated by the previous phyico-chemical characterization. Specifically and under UV illumination, previous works indicated that the contact between components of the catalysts can withdraw electrons generated from conduction band of the anatase phase after light absorption, being these carriers involved in an anihilation process with holes created at the tungstate component [8,43,44]. This de-excitation channel evidences a “Z enhancement scheme” mimicking nature photo synthesis and leaves holes at the highly active anatase surface to generate chemistry. This UV-triggered channel could be responsible of decreasing charge carrier recombination rendering an enhancement ratio of 2.6. We also detect an enhancement ratio of 3.5 upon sunlight-type illumination.

The electron capture hypothesis by the heteropolytungstate species and the subsequent influence in charge handling can be sustained by photoluminescence experiments. The Fig. 11 displays the photoluminescence results under UV and sunlight-type irradiation conditions. All samples show similar spectra, which are dominated by a band around 450 nm under UV excitation and a decay feature under visible light excitation. Both facts are typical of samples dominated by titania [45,46]. A qualitative correlation between maximum activity (maximum photonic efficiency) and lower photoluminescence becomes evident form Fig. 11, regardless of the nature of illumination, indicating a positive effect on charge carrier recombination.

As discussed earlier, the improvement of the activity is lower under UV than sunlight-type irradiation. This suggests that in addition to a positive effect from UV photons of sunlight, a specific, visible-light related contribution generated by interface effects is playing an important role in boosting the photo-catalytic performance of the samples. According to previous results [17,18,44], this is done by the larger oxidation power (leading to a most efficient oxygen capture at the surface) of the visible-excited polytungstenate anion. This new channel, which may be also operative under UV illumination, seems in any case to provide the basis for the “excess” enhancement at sunlight vs. UV illumination. The enhancement factors upon UV and visible light illumination (2.6 and 3.5) are clearly competitive with W-containing oxide species supporting in titania [23,33,38], indicating the goodness of these materials and their potential to improve the performance of any bare anatase catalyst.

On the other hand, both UV and visible light enhancement channels render maximum activity enhancement for the 20 wt. % sample. An activity maximum for a relatively high load of the heteropolytungstate has been also observed in the liquid phase photo-degradation of phenol

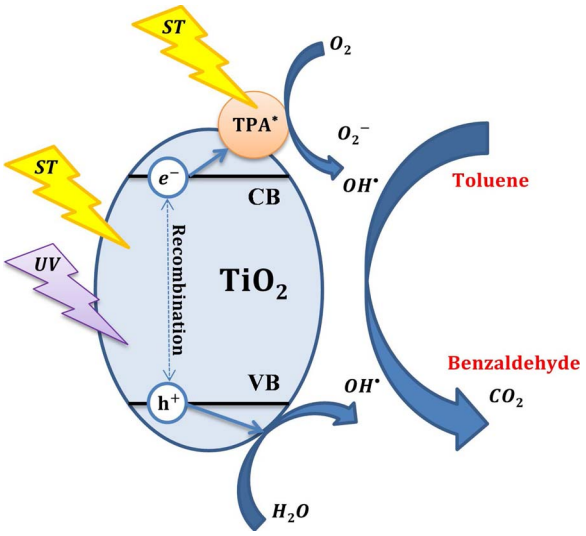

Scheme 1. Schematic representation of the main electronic events occurring after light irradiation (UV and Sunligth-type) and having an impact in the photodegradation of toluene.

[18]. The trade off between the beneficial and detrimental effects leading to an activity maximum in our composite systems has been shown to be optimized for a concentration close to the one here obtained in the case of partial photo-oxidation of 2-propanol [20]. This optimum interaction between components would optimize charge separation and minimize recombination effects in activity. For the case of sunlight-type illumination, although as described previously the activity enhancement is a combination of at least two different positive effects, the differences in oxygen activation by the different polytungstate anions presented at the anatase surface may play a key role by facilitating the attack to the different intermediates produced during the oxidation process. This reasoning has been summarized in Scheme 1 which provides a graphical representation of the main light excitation channels and the corresponding charge carrier species formed and leading to high activity in the composite system. Note that both phases generate active charge species attacking the organic molecule.

To further analyze the photo-activity evolution through the composite sample series, in Fig. 12 (and Fig. S11) we presented a comparison between two different NMR factors that can be correlated with the activity, more specifically with the apparent quantum efficiency ratio between the composite sample and the TiO_2 reference. First of all, Fig. 12A presents a comparison between the fraction of the $[PW_{11}O_{39}]^{7-}$ species (over total polytungstate concentration) estimated from NMR vs. the above mentioned apparent quantum efficiency ratio obtained under UV excitation. A strong correlation in the behavior showed by these two observables becomes evident from the plot. The absence of the $[PW_{11}O_{39}]^{7-}$ species (sample TiO_2 TPA10) produces a rather mild effect on photo-activity (the apparent quantum efficiency ratio has a rather close to unit value in Fig. 12A) while maximum activity is associated with maximum relative content of such species at the surface of titania.

On the other hand, under UV-visible irradiation (sunlight-type) conditions and according with previous studies in which tungstophosphoric acid have been immobilized on Y and ZSM5 ammonium zeolites (non-photocatalytic support), the activity of samples can be correlated with the $[PW_{12}O_{40}]^{3-}/([PW_{12}O_{40}]^{3-} + [P_2W_{21}O_{71}]^{6-}$ ratio [47]. This ratio takes accounts the relative fraction of one species among the two present in all samples of the study (including TiO_2 TPA10). The polytungstate role could be generically most relevant under sunlight than UV illumination due to the heteropolyacid excitation by visible light (a fact explained in the introduction section and graphically described in Scheme 1). Indeed, in Fig. 12B we observed (contrarily to Fig. 12A) an

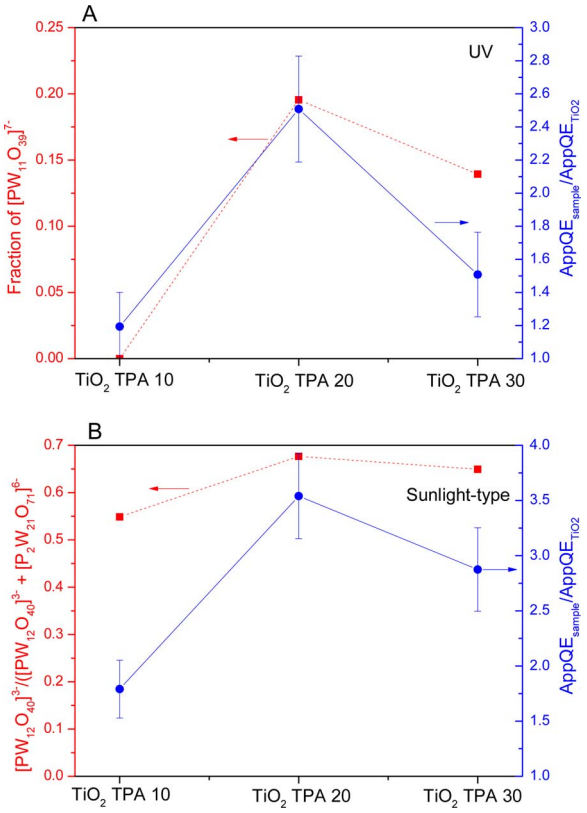

Fig. 12. Fraction of $[PW_{11}O_{39}]^{7-}$ and $[PW_{12}O_{40}]^{3-}/([PW_{12}O_{40}]^{3-} + [P_2W_{21}O_{71}]^{6-})$ vs increase over the TiO_2 reference of apparent quantum efficiency, for A: under UV irradiation and B: under sunlight-type irradiation, respectively, as a function of the polytunstate content of the materials.

enhancement of activity for all samples with respect to the bare titania reference. We can thus suggest a pivotal catalytic role of one of two species present in all catalysts under sunlight-type illumination. For such reason, in Fig. 12B we present a relative good correlation between the above mentioned factor and the increase over the apparent quantum efficiency of the TiO_2 reference. The similar trends of the two observables displayed in Fig. 12B indicate that maximum activity can be associated with the maximum relative content of $[PW_{12}O_{40}]^{3-}$anion in contact with titania.

We note, in any case, that although the above UV and sunlight-type mentioned correlations point out the importance of specific species polytungstate species in driving to an optimum activity in the degradation of toluene, this does not mean that activity is exclusively associated to one of such species. In fact, the existence at the titania surface of tungstophosphoric acid species provides the basis for a more efficient toluene photo-oxidation, irrespective of the excitation wavelength, as clearly demonstrated by the photoluminescence experiments.The interaction between the two components of the solids seems at the origin of both physical phenomena previously mentioned; the charge separation leading to a lowering of the recombination and the formation of the reduced polytungstate species. All polytungstate species seems to contribute to such effects, although likely with differences in their importance, as shown by the catalytic and spectroscopic results summarized in Fig. 12.

6. Conclusions

A series of $H_3PW_{12}O_{40}$–TiO_2 composite catalysts were synthesized by a sol-gel method and subjected to physico-chemical examination using a multitechnique approach. This study indicated the presence of three different polytungstate species at the surface of the titania oxide.

The unmodified $[PW_{12}O_{40}]^{3-}$ anion is the dominant species with little interaction with anatase. The dimeric $[P_2W_{21}O_{71}]^{6-}$ species is detected accompanying the unperturbed one from the initial concentration tested. For loadings above 10 wt. %, the additional presence of the $[PW_{11}O_{39}]^{7-}$ anion is detected.

The photo-activity of the composite and bare titania materials was evaluated for toluene photo-oxidation under UV and sunlight-type illumination. The physico-chemical characterization of the samples provides evidence that the activity enhancement observed is closely associated to the presence of different species at the titania surface, being especially relevant; the $[PW_{11}O_{39}]^{7-}$ and $[PW_{12}O_{40}]^{3-}$ anions, for respectively UV and sunlight type irradiation conditions. The effect of such species in charge handling and oxidant species appears critical to enhance both the activity and selectivity to the partial oxidation product presented by the bare anatase. In such way, the system containing a 20 wt. % of the polytungstate renders a highly activity and selective material in toluene photo-transformation.

Acknowledgements

Financial support from CSIC is fully tanked. The author L.R. Pizzio acknowledges L. Osiglio for their experimental contribution and CONICET (PIP 628) and UNLP (X638 and X732) for the financial support.

Appendix A. Supplementary data

Supplementary data associated with this article can be found, in the online version, at https://doi.org/10.1016/j.apcatb.2017.11.055.

References

[1] A. Kubacka, M. Fernández-García, G. Colón, Chem. Rev. 112 (2012) 1555–1614.
[2] J.C. Colmenares, R. Luque, Chem. Soc. Rev. 43 (2014) 765–778.
[3] O. Fontelles-Carceller, M.J. Muñoz-Batista, E. Rodríguez-Castellón, J. Carlos Conesa, M. Fernández-García, A. Kubacka, J. Catal. 347 (2017) 157–169.
[4] Q. Shen, X. Huang, J. Liu, C. Guo, G. Zhao, Appl. Catal. B 201 (2017) 70–76.
[5] Q. Shen, Z. Chen, X. Huang, M. Liu, G. Zhao, Environ. Sci. Technol. 49 (2015) 5828–5835.
[6] M.J. Muñoz-Batista, O. Fontelles-Carceller, M. Ferrer, M. Fernández-García, A. Kubacka, Appl. Catal. B 183 (2016) 86–95.
[7] M.T. Pope, A. Muller, Angew. Chem. Int-Ed. 30 (1991) 34–48.
[8] R. Sivakumar, J. Thomas, M.J. Yoon, J. Photochem. Photobiol. C 13 (2012) 277–298.
[9] Q. Zhang, Y. Tan, G. Liu, J. Zhanga, Yizhuo Han, Green Chem. 16 (2014) 4708–4715.
[10] Y. Yang, Q. Wu, Y. Guo, C. Hu, E. Wang, J Mol Catal A 225 (2005) 203–212.
[11] K. Li, Y. Guo, F. Ma, H. Li, L. Chen, Y. Guo, Catal. Commun. 11 (2010) 839–843.
[12] Y. Tamasa, Catal. Surf. Asia 7 (2003) 203–217.
[13] S. Zhang, L. Chen, H. Liu, W. Guo, Y. Yang, Y. Guo, M. Huo, Chem. Eng. J. 200–202 (2012) 300–309.
[14] R.R. Ozer, J.L. Ferry, Environ. Sci. Technol. 35 (2001) 3242–3246.
[15] M. Yoon, J.A. Chang, Y. Kim, J.R. Choi, K. Kim, J.L. Lee, J. Phys. Chem. B 105 (2001) 2539–2546.
[16] Y. Yang, Y. Guo, G. Hu, Y. Wang, Appl. Catal. A 273 (2004) 201–210.
[17] V.M. Fuchs, L. Méndez, M.N. Blanco, L.R. Pizzio, Appl. Catal. A 358 (2009) 73–78.
[18] M. Blanco, L. Pizzio, Appl. Catal. A 405 (2011) 69–78.
[19] S.-H. Li, S. Liu, J.C. Colmenares, Y.-J. Xu, Green Chem 18 (2016) 594.
[20] E.I. García-López, G. Marchí, F.R. Pomilla, G. Krpsza, A. Mineck-Iluckla, L. Palmisano, Appl. Catal. B 189 (2016) 252–265.
[21] Y. Zhang, G. Zhao, Y. Zhang, X. Huang, Green Chem. 16 (2014) 3860–3869.
[22] A. Le Bail, H. Duroy, J.L. Forquet, Mater. Res. Bull. 23 (1988) 447–452.
[23] A. Kubacka, G. Colón, M. Fernández-García, Appl. Catal. B 95 (2010) 238–244.
[24] S.E. Braslavsky, A.M. Braun, A.E. Cassano, A.V. Emeline, M.I. Litter, L. Palmisano, V.N. Parmon, N. Serpone, Pure Appl. Chem. 83 (2011) 931–1014.
[25] M. Fernández-García, X. Wang, C. Belver, J.C. Hanson, J.A. Rodriguez, J. Phys. Chem. C 111 (2007) 674–682.
[26] Y. Xiao-Feng, W. Nian-Zu, H. Hui-Zhong, X. You-Chang, T. You-Qi, J. Mater. Chem. 11 (2001) 3337–3342.
[27] H. Yang, D. Zhang, L. Wang, Mater. Lett. 57 (2002) 674–678.
[28] M. Fernández-García, A. Martínez-Arias, J.C. Hanson, J.A. Rodríguez, Chem. Rev. 104 (2004) 4063–4105.
[29] V.M. Fuchs, E.L. Soto, M.N. Blanco, L.R. Pizzio, J. Colloid Interface Sci. 327 (2008) 403–411.
[30] K. Li, X. Yang, Y. Guo, F. Ma, H. Li, L. Chen, Y. Guo, Appl. Catal. B 99 (2010) 364–375.
[31] C.D. Wagner, W.M. Riggs, L.E. Davis, J.F. Moulder, G.E. Muilenber (Ed.), Handbook of X-ray Photoemission spectra, Perkin-Elmer, Minnesota, 1976.
[32] A. Kubacka, M. Fernández-García, G. Colón, J. Catal. 254 (2008) 272–284.
[33] A. Kubacka, B. Bachiller-Baeza, G. Colón, M. Fernández-García, J. Phys. Chem. C 113 (2009) 8553–8555.
[34] C. Rocchiccioli-Deltcheff, R. Thouvenot, R. Franck, Spectrochim. Acta 32 (1976) 587–597.
[35] M. Fernández-García, C. Belver, J.C. Hanson, X. Wang, J.A. Rodríguez, J. Am. Chem. Soc. 129 (2007) 13604–13612.
[36] R. Massart, R. Contant, J. Fruchart, J. Ciabrini, M. Fournier, Inorg. Chem. 16 (1977) 2916–2921.
[37] V.M. Mastikhin, S.M. Kulikov, A.V. Nosov, I.V. Kozhevnikov, I.L. Mudrakovsky, M.N. Timofeeva, J. Mol. Catal.A: Chem 60 (1990) 65–70.
[38] M.J. Muñoz-Batista, R. Rachwalick, B. Bachiller-Baeza, A. Kubacka, M. Fernández-García, J. Catal. 309 (2014) 428–438.
[39] G. Marcí, M. Addamo, V. Augugliaro, S. Coluccia, V. Loddo, G. Matra, L. Palmisano, M. Schiavello, J. Photochem. Photobiol. A 160 (2003) 105–114.
[40] T. Guo, Z. Dai, C. Wu, T. Zhu, Appl. Catal. B 79 (2008) 171–178.
[41] M. Sleiman, P. Conchon, C. Ferronato, J.-M. Chovelon, Appl. Catal. B 86 (2009) 159–165.
[42] U. Caudillo-Flores, M.J. Muñoz-Batista, F. Ung-Medina, G. Alonso-Núñez, A. Kubacka, J.A. Cortés, M. Fernández-García, Chem. Eng. J. 299 (2016) 393–402.
[43] H. Park, W. Choi, J. Phys. Chem. B 107 (2003) 3885–3890.
[44] S. Yanagida, A. Nakajima, T. Sasaki, Y. Kameshima, K. Okada, Chem. Mater. 20 (2008) 3757–3764.
[45] M.J. Muñoz-Batista, U. Caudillo-Flores, F. Ung-Medina, Ma. del Carmen Chávez-Parga, J.A. Cortés, A. Kubacka, M. Fernández-García, Appl. Catal. B 201 (2017) 400–410.
[46] M.J. Muñoz-Batista, A. Kubacka, O. Fontelles-Carceller, D. Tudela, M. Fernández-García, ACS Appl. Mater. Interfaces 8 (2016) 13934–13945.
[47] C.L. Marchena, R.A. Frenzel, S. Gomez, L.B. Pierella, L.R. Pizzio, Appl. Catal. B 130-131 (2013) 187–196.